Nanotechnology **19** (2008) 424018 (8pp) doi:10.1088/0957-4484/19/42/424018

Spray-deposited $CuInS_2$ solar cells

Albert Goossens and Joris Hofhuis

Opto-Electronic Materials, Delft University of Technology, Julianalaan 136, 2628 BL Delft, The Netherlands

Received 23 April 2008, in final form 30 June 2008
Published 25 September 2008
Online at stacks.iop.org/Nano/19/424018

Abstract

Spray deposition of $CuInS_2$ offers an attractive route towards industrial production of thin-film solar cells. With spray deposition it is possible to make nanocomposites of n-type TiO_2 and p-type $CuInS_2$. Upon application of an In_2S_3 buffer layer, solar cells can be made with efficiencies of ∼7%, being comparable to that of amorphous silicon. Rapid thermal annealing is not involved in the production of these solar cells. In order to further improve the performance, the concentration of electronic defect states in the bandgap must be reduced. Towards this end a detailed study has been undertaken to elucidate the role of associated point defects in the recombination of electron–hole pairs. Especially with transient absorption spectroscopy it is possible to make an accurate assessment of the fundamental electronic processes that are involved. We find electronic states in the bandgap related to the presence of anti-site defects. In addition, indium vacancies are also involved. State-to-state recombination occurs, indicating that the involved defects are associated. An electronic state located at 1.1 eV above the valence band, which is related to indium on a copper position, has a lifetime of about 20 μs at room temperature. The lower lying states related to copper on indium positions, and indium vacancies, are populated from this 1.1 eV state.

(Some figures in this article are in colour only in the electronic version)

1. Introduction

Despite the enormous growth of the solar cell market, the present solar cell technology needs to be replaced by cheaper and better ones in the near future. To that end, third-generation cells are being investigated across the globe. Pioneering research in the groups of Grätzel [1–4] and Heeger [5, 6] have shown that solar cells based on nanostructured and nanocomposite materials can indeed be made. From these discoveries new approaches to solar cell research and technology have emerged, which are now further explored and tested on a laboratory and small industrial scale.

Common to Grätzel's 'dye-sensitized' and Heeger's 'bulk heterojunction' solar cells is the occurrence of light absorption in close proximity to the active interface, where exciton separation occurs. In fact, the photoactive area is reduced to one monolayer of light absorbing dye in a Grätzel cell and to a few nanometers in a bulk heterojunction cell. After light absorption and exciton separation have taken place, carrier collection remains to be done. In dye cells, electrons percolate through the sintered nanoporous TiO_2 electrode and holes are transported by a liquid redox electrolyte. In bulk heterojunction cells, electrons tunnel between the C_{60} molecules, that make up most of the volume, while holes are transported in the light absorbing polymer.

Inspired by these new solar cell architectures, several variations have been elaborated to obtain an all-solid nanocomposite solar cell. The reason for this research is that for dye and polymer cells encapsulation must be extremely good to warrant a reasonable lifetime. When operating in full sunlight and with standard humidity, dye cells and polymer cells degrade fast, unless excellent sealing is applied. The need for such expensive sealing adds considerable complexity to the production of these cells, which challenges the necessary cost reduction. Therefore, all-solid nanocomposite cells are desirable, as the sealing requirements for these cells are much less stringent.

Pioneering work towards all-solid nanocomposite cells was delivered by O'Regan [7] and Tennakone [8], who still used molecular light absorbing dyes but replaced the redox electrolyte with a transparent inorganic hole conductor, such as CuI and CuSCN. At the Hahn Meitner Institute (HMI) Rolf Könenkamp introduced the 'extremely thin absorber' (ETA) cell [9–12]. In this design, stable inorganic compounds replace all non-solid components of a dye cell. As the nanostructured electron transporting material, either TiO_2 or ZnO is used, being nanoporous or present as nanowires or nanotubes. Light absorption takes place by visible light absorbing semiconductors, such as CdTe, ZnTe and $CuInS_2$.

Finally, hole transport is taken care of by a wide-bandgap p-type semiconductor (CuI or CuSCN). Outside the HMI, ETA cells have also been investigated elsewhere [13, 14].

In our laboratory at TU Delft the bulk heterojunction concepts have been followed rather than the ETA concept. In the TU Delft so-called 3D solar cells, visible light absorption and hole transport takes place in a single material. This material is applied inside the voids of a nanoporous wide-bandgap electron conductor. The materials that give the best results are anatase TiO_2 as the nanoporous electron conductor and $CuInS_2$ as the visible light absorber and hole conductor. In order to obtain such a 3D nanocomposite cell, two ways of depositing $CuInS_2$ inside the voids of nanoporous TiO_2 have been developed, i.e. atomic layer deposition (ALD) and spray deposition. Without a buffer layer, operating solar cells can be obtained albeit with low energy conversion efficiency. The reason for this low efficiency is the large density of electronic interface states at the $TiO_2|CuInS_2$ junction. These states lie in the bandgap of $CuInS_2$ and promote the back flow of electrons, i.e. they create an electronic shunt. A buffer layer needs to be applied to avoid shunting of the photocurrent. Both CdS and In_2S_3 can be applied, and in lieu of the environmental issues related to the use of cadmium, we have chosen to focus on In_2S_3 buffer layers only. Another advantage of In_2S_3 over CdS is its slightly larger bandgap. Detailed investigations of the interface between TiO_2 and $CuInS_2$ as well as on the role of the buffer material can be found in [15, 16].

The atomic layer deposition technique is uniquely qualified to infiltrate porous materials and indeed 3D nanocomposites of TiO_2 and $CuInS_2$ with In_2S_3 as the buffer can be obtained [17–21]. With Rutherford backscattering and grazing incidence XRD it has been shown that infiltration of nanoporous TiO_2 is possible, although absolute numbers of the void fraction after infiltration have not been obtained [19]. The possible lack of full infiltration is, however, not critical to the operation for a 3D solar cell.

While atomic layer deposition is the method of choice to infiltrate porous materials, the maximum deposition rate is small, which may hinder rapid industrial production of large panels. Therefore, we replaced the ALD process with a much more convenient deposition method. Spray deposition came out as the most successful one and the present paper deals only with spray-deposited cells. The deposition method will briefly be introduced. The main focus of the present work is to discuss the material quality, since that is a critical factor for obtaining solar cells with good conversion efficiencies.

2. Spray-deposited solar cells

The use of spray deposition to obtain $CuInSe_2$-based solar cells had been initiated in 1982. These cells showed a disappointing low conversion efficiency of about 2% [22, 23]. However, research continued, especially at the Tallinn Technical University, where Malle Krunks advanced spray deposition of CIS by carefully studying the chemistry involved [24–30]. When we came into contact with this group it was realized that spray deposition could be a good choice to replace the ALD deposition process. And, indeed, this showed to be the case.

In spray deposition of CIS, an aqueous solution of $CuCl_2$, $InCl_3$ and thiourea is prepared and fed to an atomizer. We have used glass nebulizers based on the ventura principle, but other nebulizers can be applied as well. The droplet size is a critical parameter, as will be further discussed below. The glass samples are placed on a hot plate in air with a surface temperature around 300 °C. The surface temperature is critical and should be uniform over the sample. Finally one should carefully consider the distance between the nozzle of the nebulizer and the hot surface of the samples.

Immediately after their formation the droplets start to evaporate. At a certain point supersaturation occurs, leading to the formation of a solid deposit inside the droplet. Different deposition regimes can occur. If the distance between the nozzle and the hot surface is large, solid nanoparticles form and precipitate onto the hot surface, where they are sintered to form a nanoporous film. This deposition regime yields non-uniform films with poor adhesion and cannot be applied for solar cells. If the distance between the nozzle and the hot surface is made smaller one can enter the regime at which the droplets have not fully evaporated yet and precipitate, like rain, onto the surface. There the droplets coalesce and evaporate, from which big lumps of CIS crystallize. Also these films are not good, since the adhesion is poor and usually many pinholes are formed. The desired deposition regime lies between these two extremes. Since many parameters are involved careful fine-tuning of the process is required.

Owing to its potential for large-scale application on an industrial scale, spray deposition of $CuInS_2$ finds increasing interest [31–37] and has become an important research topic in our group [38–42].

The spray deposition method is further elaborated at Advanced Surface Technology (AST), aiming towards solar cells in which all thin-film components, i.e. the transparent conducting oxide, the anatase TiO_2, the In_2S_3 buffer and the $CuInS_2$ light absorber, are obtained with spray deposition in air. In their process only 98% pure chloride precursors are used, which makes the whole production process very attractive. Indeed a production cost prize of 0.4 €/Wp is anticipated. At the AST facility fully sprayed CIS solar cells with a conversion efficiency of 7% and a size of 12 cm × 10 cm are made, which indeed shows the great potential for this new technology. Figure 1 shows i–V curves of fully spray-deposited cells, in the dark and with simulated AM1.5 irradiation.

Despite the encouraging results that have been obtained so far there is still room for improvement. For instance, the open-circuit voltage of ∼0.7 V is not more than half the 1.55 eV bandgap of CIS. To improve this situation the loss factors need to be known. To that end the optical and electronic properties of spray-deposited CIS have been investigated in depth. This will be the focus of the present study.

3. Experimental aspects

3.1. Spray deposition

For our optical studies, $CuInS_2$ samples have been prepared by AST on quartz substrates using spray deposition in ambient

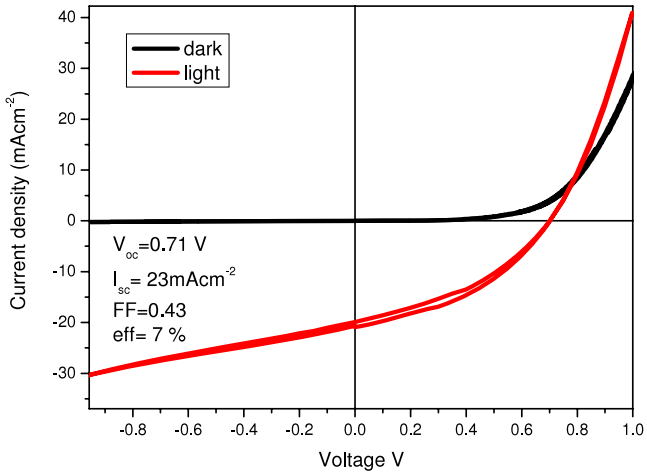

Figure 1. Current–voltage response of fully spray-deposited $CuInS_2$ and In_2S_3 onto TiO_2. The irradiation source is a calibrated solar simulator with AM1.5 (1000 W m^{-2}) emission.

atmosphere. An automatic spray robot is used to deposit a thin layer of $CuInS_2$ onto 2 mm thick quartz substrates, which are cleaned first by successive immersion in acetone and ethanol in an ultrasonic bath. $CuCl_2{\cdot}2H_2O$ (98% Aldrich), $InCl_3$ (98%, Aldrich) and thiourea (98%, Aldrich) dissolved in purified water have been used for spray deposition of $CuInS_2$. The composition of the solution is such that Cu-rich material is formed. The best results are obtained if the deposition temperature is maintained at 300 °C. The film thickness is controlled by the number of sprays, which has been varied between 10 and 20.

3.2. Photoluminescence spectroscopy

Photoluminescence measurements are performed in backscatter mode. The sample is mounted in a closed-cycle helium cryostat (APD Cryogenics CSW-204sl) and cooled to 10 K. Excitation occurs by a Nd:YVO_4 laser, operating at a wavelength of 532 nm (SpectraPhysics Milennia) with 200 mW power. Neutral density filters are used to vary the laser power. The excitation wavelength is removed from the PL signal by a notch filter (Kaiser) and a 620 nm Schott filter. An optical fiber carries the signal to a monochromator (Acton SpectroPro 2500i). The spectrum is recorded by a liquid-nitrogen-cooled CCD array (Princeton Instruments LN/CCD-1100PB) for the visible range, or a liquid-nitrogen-cooled InGaAs detector (Princeton Instruments OMA-V) for the NIR range. PL measurements are integrated over 60 s.

3.3. Transient absorption

The transient absorption (TA) set-up includes a low-intensity probe beam, obtained from a halogen lamp (Oriel) and a monochromator (Acton SpectroPro 150), that irradiates the sample with a small solid angle. The transmitted beam is focused into a second monochromator (Acton SpectroPro 150). Silicon and InGaAs photodiodes are used as detectors. The electrical signal is amplified (Femto HCA-200M-20K-C) and recorded with an oscilloscope (Tektronix TDS 744). The

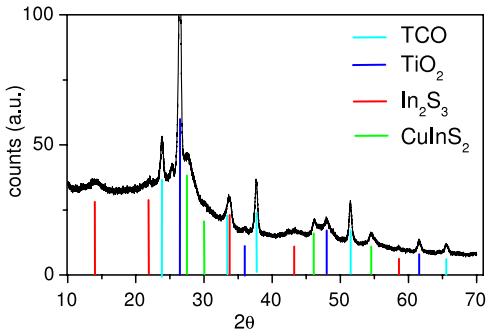

Figure 2. X-ray diffraction of a spray-deposited $CuInS_2|In_2S_3|TiO_2$ solar cell.

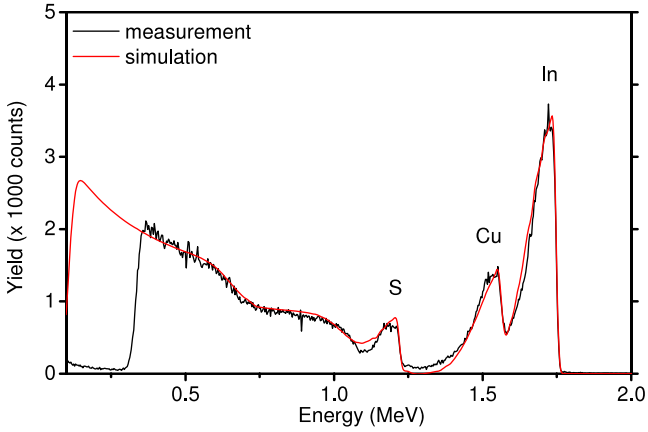

Figure 3. Rutherford backscattering of spray-deposited $CuInS_2$. The close match between the experimental data and the simulated response is an indication of the good quality of $CuInS_2$ with regard to elemental composition.

pulse beam is generated by a Nd:YAG laser (SpectraPhysics QCR) operating at 10 Hz repetition rate, which pumps an optical parametric oscillator (SpectraPhysics MOPO 710) where 532 nm pulses with a duration of 5 nm are made. After passing through neutral density filters the energy of the pulse is 4 μJ/pulse.

4. Results

4.1. Material characterization

Spray-deposited $CuInS_2$ has the nominal chalcopyrite crystal structure. In figure 2, an x-ray diffraction (XRD) spectrum of a complete solar cell, i.e. $CIS|In_2S_3|TiO_2|TCO$ is shown. All XRD peaks are narrow and belong to one of the materials involved. Other materials or phases have not been found. In addition to XRD, Rutherford backscattering (RBS) has also been applied. With this method the stoichiometry and molecularity of CIS can be studied. As shown in figure 3, only Cu, In and S are found. The excellent match between the experimental data and the simulated response (see figure 3) is another indication of the excellent material quality that can be obtained with spray deposition. It should be noted that rapid thermal annealing is not involved in the production of these solar cells.

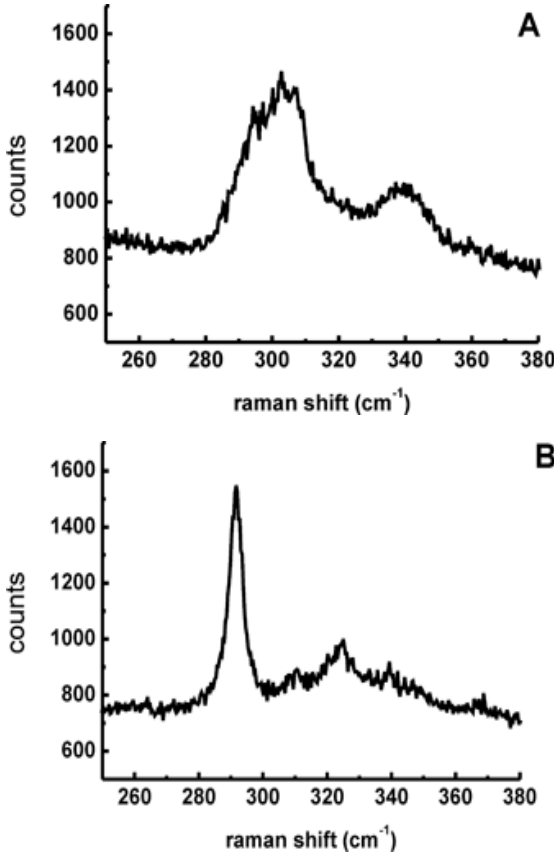

Figure 4. Raman spectrum of spray-deposited $CuInS_2$ before (A) and after (B) rapid thermal annealing.

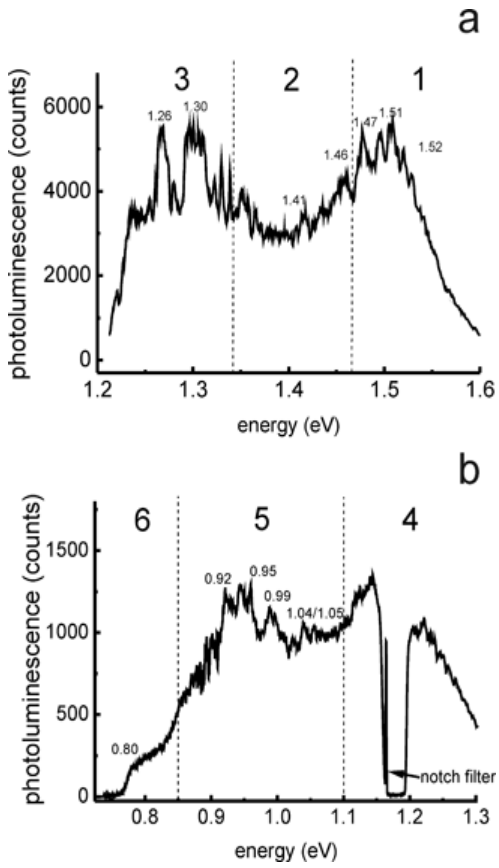

Figure 5. Photoluminescence spectrum of as-deposited $CuInS_2$ in the visible (a) and near-infrared region (b). The spectra are recorded at 10 K.

With regard to the morphology it is difficult to make a quantitative assessment. The droplet size shows some variation, leading to rough CIS films with a large variety of morphologies. Clearly the CIS and In_2S_3 phases interpenetrate to form a nanocomposite. However, the exact morphology that is obtained shows a large variety. Current investigations are directed to elucidate the morphological structure in more detail.

For the present investigations $CuInS_2$ is applied onto quartz since this guarantees that the photoluminescence and transient absorption signals originate exclusively from $CuInS_2$ and not from any other material.

4.2. Raman spectroscopy and photoluminescence

With Raman spectroscopy, convoluted peaks are found at 293 and 305 cm^{-1} with an FWHM linewidth of $\sim$10 cm^{-1}. The peak positions and widths match with the literature [43–45]. A typical Raman spectrum for as-deposited CIS is shown in figure 4(a). For comparison, a Raman spectrum after rapid thermal annealing is also shown (figure 4(b)). However, the present investigation concerns only non-annealed $CuInS_2$. Following the findings of Alvarez-García [43, 44], Riedle [45] and Rudigier [55] Raman peak broadening is related to the presence of associated point defects. Indeed, associated point defect formation is expected in spray-deposited CIS. To further investigate the nature of these defects, detailed photoluminescence (PL) and transient absorption (TA) studies have been undertaken. A typical PL spectrum recorded at 10 K is shown in figure 5. Photoluminescence spectra of $CuInS_2$ reported in earlier studies are essentially similar, although the sensitivity of our set-up is higher [46–55]. In the PL spectra, families of peaks are found which should not be regarded as experimental noise. The noise level of the PL set-up is much less than the height of the peaks. Obviously, spray-deposited CIS consists of small nanoscale crystallites all having a slightly different composition and defect structure. The laser irradiates a number of crystallites which give rise to families of related PL peaks. However, upon careful examination related PL peaks can be found between 1.52 and 1.35 eV (groups 1 and 2), between 1.35 and 1.1 eV (groups 3 and 4) and between 1.1 and 0.7 eV (groups 5 and 6). Assignment of these emissions to (associated) point defects shall be discussed below.

5. Transient absorption

With transient absorption (TA) spectroscopy the charging and discharging of sub-bandgap electronic states can be observed. When this method is applied to spray-deposited CIS all PL transitions show up. Moreover, while PL only provides relative energy data, with TA it is possible to locate the involved energy states relative to the valence band. Typical TA traces

Table 1. Transient absorption results. The pre-factors indicate whether the signal is a bleach (negative pre-factor) or an absorption (positive pre-factor).

PL group no.	Probe energy (eV)	$A1 \times 10^{-3}$	$\tau 1$ (μs)	$A2 \times 10^{-3}$	$\tau 2$ (μs)	$A3 \times 10^{-3}$	$\tau 3$ (μs)
1	1.65	−13.2	0.51 ± 0.06	−2.66	5.6 ± 2.4	−1.81	40 ± 20
2	1.38	−5.00	0.40 ± 0.05	1.80	3.0 ± 0.1	1.76	30 ± 0.7
3	1.30	−2.2	0.65 ± 0.05	0.6	3.8 ± 0.5	0.94	50 ± 0.5
4	1.08	−3.73	0.22 ± 0.01			−0.32	20 ± 0.5
5	0.95	−3.45	0.36 ± 0.01			−0.85	20 ± 0.5
6	0.86	−2.3	0.50 ± 0.05			−0.84	20 ± 0.2

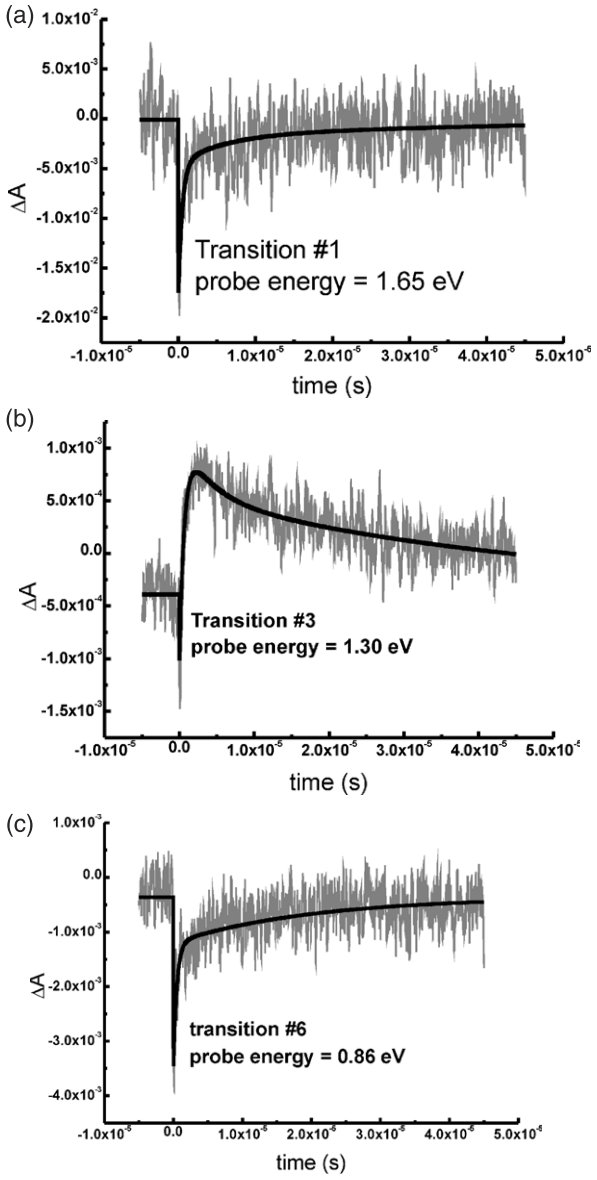

Figure 6. Transient absorption spectra recorded at different probe wavelengths. The pump wavelength is fixed at 532 nm.

are shown in figures 6(a)–(c). In addition to the energy positions of sub-bandgap electronic states, their occupation dynamics can also be derived from TA experiments. The absorption transients along with their lifetimes are collected in table 1.

6. Discussion

The presence of shallow states in the bandgap of CIS is well documented. These states are responsible for the conduction type (n- or p-type) of CIS. Both types can be made. Obviously the donor/acceptor density has a large influence on the junction formation and determines the creation of a built-in electric field. As such they affect the photovoltage that can be generated in a CIS solar cell. However, the photocurrent is not affected much, since electron–hole recombination occurs primarily in deep electronic states, rather than via shallow ones. In spray-deposited CIS, deep electronic states are indeed found at 0.2 and 1.15 eV above the valence band. The presence of these states could lead to efficient recombination, but this does not occur since the photocurrents of spray-deposited CIS cells are quite high. The reason is that the occupation time of electrons in the 1.15 eV state is long, i.e. more than 20 μs. Another remarkable observation is that the population dynamics of the 1.15 eV state is coupled to that of the 0.2 and 0.15 states. This can only be explained if the 1.15 eV defect state is located physically in close proximity to the 0.2 and 0.15 eV defect states.

Based on previous literature data combined with our own findings we postulate the following defect structure for spray-deposited CIS. The conduction band lies at 1.55 eV and at 1.5 eV a shallow donor state due to sulfur vacancies $V_S^{\bullet\bullet}$ is found. Much lower in energy a deep donor state at 1.15 eV is present. This state is related to $In_{Cu}^{\bullet\bullet}$ and is split into two narrow-spaced levels at 1.15 and 1.1 eV. At 0.2 eV above the valence band one finds a deep acceptor state assigned to Cu_{In}''. Upon close examination also this level appears to be a doublet at 0.2 and 0.25 eV. Finally, there is another deep acceptor at 0.15 eV, which is related to indium vacancies V_{In}'''. In figure 7 the proposed energy level scheme is shown. It should be realized that this diagram only highlights the most important defect states. From the photoluminescence spectra it is clear that there are more states from which PL can occur.

The point defects introduced above are present simultaneously. Although we try to avoid reduction of CIS during the deposition process some sulfur atoms escape from the surface, leading to $V_S^{\bullet\bullet}$ formation. The concentration of $V_S^{\bullet\bullet}$ is not very high since the conductivity type of the samples is p-type. The reason is that spray deposition takes place in air. When sulfur vacancies form they are substituted immediately by oxygen, leading to $O_S{}^x$, being a neutral species. We have no indication that $O_S{}^x$ introduces an electronic state in the bandgap of CIS, making their presence quite harmless.

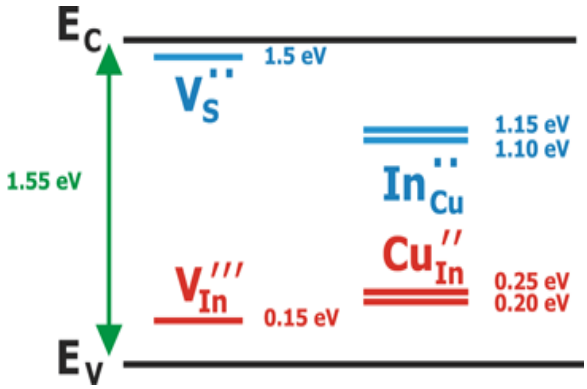

Figure 7. Energy diagram derived from PL data with sub-bandgap electronic states in $CuInS_2$.

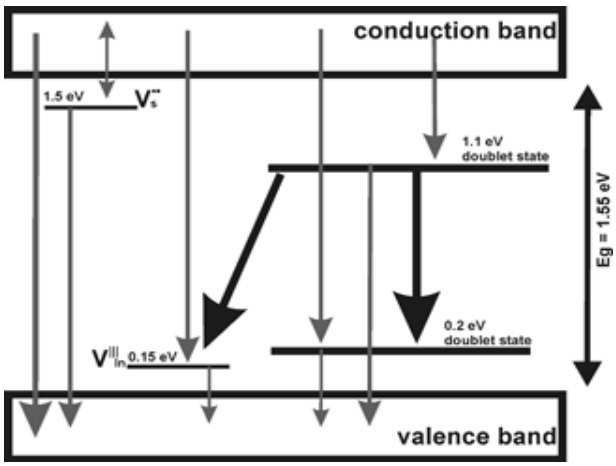

Figure 8. Energy diagram derived from TA data with the observed electron–hole recombination pathways.

Two important electronic states are closely related, i.e. $In_{Cu}^{\bullet\bullet}$ and Cu_{In}''. They are so-called anti-site defects. We observe photoemission from the conduction band to the Cu_{In}'' (0.2/0.25 eV) state and from the $In_{Cu}^{\bullet\bullet}$ (1.15/1.1 eV) state to the valence band. In addition we also observe emission between these deep donor–acceptor states. Such emission is only possible if the involved defects are in close proximity. Indeed, following the analysis by Krustok *et al*, we postulate that $In_{Cu}^{\bullet\bullet}$ and Cu_{In}'' are either nearest neighbors or next-nearest neighbors. These two possibilities gives rise to a splitting of the states, as is indeed observed. $(In_{Cu}^{\bullet\bullet} - Cu_{In}'')^x$ nearest neighbors yield electron states at 1.15 and 0.2 eV, while $(In_{Cu}^{\bullet\bullet} - Cu_{In}'')^x$ next-nearest neighbors yield electron states at 1.1 and 0.25 eV. Furthermore, we also find an optical transition between the $In_{Cu}^{\bullet\bullet}$ (1.15/1.1 eV) state and the V_{In}''' (0.15 eV) state. Apparently, these states are also in close proximity.

Based on the analysis of the PL and the TA data we conclude that V_{In}''', $In_{Cu}^{\bullet\bullet}$ and $Cu_{In'}$ are located close to each other within the same unit cell and form a so-called defect associate. To date, not much is known about defect associates in CIS or in related selenium-based compounds. The spray-deposited CIS of the present study is Cu-rich and p-type. Accordingly, copper vacancies, $V_{Cu''}$, are not present, leaving V_{In}''' as the dominant acceptor. In addition, anti-site defects have a neutral charge and can always be formed. However, to reduce the energy barrier of anti-site defect formation it is advantageous to remove the copper ion from its position by letting it occupy an indium vacancy first. Next an indium ion jumps to the vacant copper position, leaving an indium vacancy behind. The following defect formation mechanism is proposed:

$$\text{Step 1: } Cu_{Cu}^{x} + V_{In}''' \rightarrow Cu_{In}'' + V_{Cu}'$$

$$\text{Step 2: } V_{Cu}' + In_{In}^{x} \rightarrow In_{Cu}^{\bullet\bullet} + V_{In}'''.$$

In other words, anti-site disorder is preferably formed near an indium vacancy leading to a $(V_{In}''' - In_{Cu}^{\bullet\bullet} - Cu_{In}'')'''$ defect association. Indeed, the presence of these associates explains the PL and TA results of the present study.

7. $CuInS_2$ solar cells

The defect association discussed above yields electronically coupled defects, which opens a recombination path by which the solar cell efficiency decreases. It is remarkable though that, even with these defects being present, photocurrent generation is still high; sprayed CIS solar cells of 7% efficiency are obtained. This is due to the slug discharging kinetics of the 1.15/1.1 eV ($In_{Cu}^{\bullet\bullet}$) state. With transient absorption we find a decay lifetime of more than 20 μs at room temperature. The energy distance between the 1.15/1.1 eV state and the conduction band at 1.55 eV is too large to cross at room temperature. Only direct relaxation to the valence band or via the associated $(V_{In}''' - In_{Cu}^{\bullet\bullet} - Cu_{In}'')'''$ states remain. Apparently the orbital overlap in this defect cluster is not large, leading to a small transition probability.

What happens upon irradiation is that conduction band electrons are trapped at the $In_{Cu}^{\bullet\bullet}$ sites at 1.15/1.1 eV. There they stay for 20 μs which gives rise to building up of a space charge. This space-charge forming process, also called photodoping, influences the potential distribution and will also affect the position of the electron quasi-Fermi level. In figure 8 the defect-mediated electron–hole recombination pathways are schematically presented. We have strong indications, but no absolute proof, that this may be the reason for the low photovoltage that is usually found for $CuInS_2$ solar cells. In addition, the well-known crossover of the i–V curves in CIS may also find its origin in charging of the 1.15/1.1 eV defect states. Further investigations are ongoing to clarify this point.

When $CuInS_2$ is annealed at 600 °C in the presence of sulfur, the defect concentration reduces such that associated defects break up to form independent point defects. This gives rise to a sharpening of the Raman peaks to 4 cm^{-1} (figure 4(b)) and to an increase of the open-circuit voltage [55]. However, since Cu and In are mobile in $CuInS_2$ [56–58] annealing can also change the molecularity and thus the nature of the p–n junction [59]. When designing solar cells based on semiconductor nanocomposites, ionic migration becomes important. To date, not much is know about ionic migration in semiconductor nanocomposites.

8. Conclusions

With spray deposition it is possible to obtain solar cells based on $TiO_2|In_2S_3|CuInS_2$ nanostructured junctions. Since spray deposition takes place in air and requires only 98% pure chemicals, low-cost solar cells can be made on an industrial scale. Spray deposition of $CuInS_2$ introduces associated defects which are involved in the electron–hole recombination process. With transient absorption spectroscopy we find that the population lifetime of electrons in deep states is large. This implies that these states act as electron traps rather than as recombination centers. Upon irradiation, electrons are stored, leading to space–charge formation. This temporal storage of charge explains the observed low open-circuit voltage of CIS cells as well as the crossover of the current–voltage curves.

Acknowledgments

The defect chemistry of $CuInS_2$ has been a topic of discussion with Joop Schoonman, for which we want to acknowledge him kindly. In addition, the workers at Advanced Surface Technology b.v., in particular Ben Meester and Marius Nanu, have also contributed significantly to the present paper by providing us with samples, along with the i–V curves, the XRD spectrum and RBS graph. The investigations on spray-deposited $CuInS_2$ are financially supported by SenterNovem.

References

[1] O'Regan B and Grätzel M 1991 *Nature* **353** 737
[2] Bach U, Lupo D, Comte P, Moser J E, Weissörtel F, Salbeck J, Spreitzer H and Grätzel M 1998 *Nature* **395** 583
[3] Grätzel M 2000 *Handbook of Nanostructured Materials and Nanotechnology* vol 3, ed H S Nalwa (San Diego: Academic) chapter 10, pp 527–53
[4] Krüger J, Plass R, Cevey L, Piccirelli M, Grätzel M and Bach U 2001 *Appl. Phys. Lett.* **79** 2085
[5] Sariciftci N S, Smilowitz L, Heeger A J and Wudl F 1992 *Science* **258** 1474
[6] Yu G, Gao J, Hummelen J C, Wudl F and Heeger A J 1995 *Science* **270** 1789
[7] O'Regan B, Schwartz D T, Zakeeruddin S M and Grätzel M 2000 *Adv. Mater.* **12** 1263
[8] Tennakone K, Senadeera G K R, De Silva D B R A and Kottegoda I R M 2000 *Appl. Phys. Lett.* **77** 2367
[9] Rost C, Sieber I, Siebentritt S, Lux-Steiner M C and Könenkamp R 1999 *Appl. Phys. Lett.* **75** 692
[10] Ernst K, Engelhardt R, Ellmer K, Kelch C, Muffler H-J, Lux-Steiner M Ch and Könenkamp R 2001 *Thin Solid Films* **387** 26
[11] Kaiser I, Ernst K, Fischer Ch-H, Könenkamp R, Rost C, Sieber I and Lux-Steiner M Ch 2001 *Sol. Energy Mater. Sol. Cells* **67** 89
[12] Ernst K, Belaidi A and Könenkamp R 2003 *Semicond. Sci. Technol.* **18** 475
[13] Lévi-Clément C, Katty A, Bastide S, Zenia F, Mora I and Munoz-Sanjose V 2002 *Physica* E **14** 229
[14] Lévi-Clément C, Tena-Zaera R, Ryan M A, Katty A and Hodes G 2005 *Adv. Mater.* **17** 1512
[15] Savenije T J, Nanu M, Schoonman J and Goossens A 2007 *J. Appl. Phys.* **101** 113718
[16] Hofhuis J, Schoonman J and Goossens A 2008 *J. Appl. Phys.* **103** 14503
[17] Reijnen L, Meester B, Goossens A and Schoonman J 2002 *Mater. Sci. Eng.* C **19** 311–4
[18] Nanu M, Reijnen L, Meester B, Goossens A and Schoonman J 2003 *Thin Solid Films* **431/432** 492–6
[19] Reijnen L, Feddes B, Vredenberg A M, Schoonman J and Goossens A 2004 *J. Phys. Chem.* B **108** 9133–7
[20] Nanu M, Reijnen L, Meester B, Schoonman J and Goossens A 2004 *Chem. Vapor Depos.* **10** 45–9
[21] Nanu M, Schoonman J and Goossens A 2004 *Adv. Mater.* **16** 453–6
[22] Bates C W, Nelson K F, Atiqraza S, Mooney J B, Recktenwald J M, Macintosh L and Lamoreau R 1982 *Thin Solid Films* **88** 279–83
[23] Tomar M S and Garcia F J 1982 *Thin Solid Films* **90** 419–23
[24] Krunks M, Bijakina O, Varema T, Mikli V and Mellikov E 1999 *Thin Solid Films* **338** 125–30
[25] Krunks M, Mikli V, Bijakina O, Rebane H, Mere A, Varema T and Mellikov E 2000 *Thin Solid Films* **361** 61–4
[26] Krunks M, Leskela T and Niinisto L 2000 *Japan. J. Appl. Phys.* **39** 181–6
[27] Krunks M, Bijakina O, Mikli V, Rebane H, Varema T, Altosaar M and Mellikov E 2001 *Sol. Energy Mater. Sol. Cells* **69** 93–8
[28] Krunks M, Kijatkina O, Rebane H, Oja I, Mikli V and Mere A 2002 *Thin Solid Films* **403** 71–5
[29] Kijatkina O, Krunks M, Mere A, Mahrov B and Dloczik L 2003 *Thin Solid Films* **431/432** 105–9
[30] Kijatkina O 2004 Deposition of copper indium disulphide films by chemical spray pyrolysis *PhD Thesis* Tallinn Technical University
[31] Hollingworth J A, Buhro W E, Hepp A F, Jenkins P P and Stan M A 1998 *Mater. Res. Soc. Symp. Proc.* **495** 171–6
[32] Hollingworth J A, Hepp A F and Buhro W F 1999 *Chem. Vapor Depos.* **5** 105–8
[33] Bouzouita H, Bouguila N and Dhouib A 1999 *Renew. Energy* **17** 85–93
[34] Zouaghi M C, Ben Nasrallah T, Marsillac S, Bernède J C and Belgacem S 2001 *Thin Solid Films* **382** 39–46
[35] Marsillac S, Zouaghi M C, Bernède J C, Ben Nasrallah T and Belgacem S 2003 *Sol. Energy Mater. Sol. Cells* **76** 125–34
[36] John T T, Mathew M, Kartha C S, Vijayakumar K P, Abe T and Kashiwaba Y 2005 *Sol. Energy Mater. Sol. Cells* **89** 27–36
[37] John T T, Kartha C S, Vijayakumar K P, Abe T and Kashiwaba Y 2006 *Appl. Phys.* A **82** 703
[38] Oja I, Nanu M, Katerski A, Krunks M, Mere A, Raudoja J and Goossens A 2005 *Thin Solid Films* **480** 82–6
[39] Nanu M, Schoonman J and Goossens A 2005 *Adv. Funct. Mater.* **15** 95–100
[40] Nanu M, Schoonman J and Goossens A 2005 *Nano Lett.* **5** 1716–9
[41] O'Hayre R, Nanu M, Schoonman J, Goossens A, Wang Q and Grätzel M 2006 *Adv. Funct. Mater.* **16** 1566–76
[42] O'Hayre R, Nanu M, Schoonman J and Goossens A 2007 *Nanotechnology* **18** 55702
[43] Alvarez-Garcia J, Marcos-Ruzafa J, Perez-Rodriguez A, Romano-Rodriguez A, Morante J R and Scheer R 2000 *Thin Solid Films* **361** 208–12
[44] Alvarez-Garcia J, Perez-Rodriguez A, Romano-Rodriguez A, Morante J R, Calvo-Barrio L, Scheer R and Klenk R 2001 *J. Vac. Sci. Technol.* A **19** 232–9
[45] Thomas R 2002 Raman spectroscopy for the analysis of thin $CuInS_2$ films *PhD Thesis* Technical University of Berlin
[46] Binsma J J M, Giling L J and Bloem J 1982 *J. Lumin.* **27** 35–53
[47] Binsma J J M, Giling L J and Bloem J 1982 *J. Lumin.* **27** 55–72
[48] Ueng H Y and Hwang H L 1989 *J. Phys. Chem. Solids* **50** 1297–305
[49] Wakita K, Nishi K, Ohta Y and Nakayama N 2002 *Appl. Phys. Lett.* **80** 3316
[50] Krustok J, Schon J H, Collan H, Yakushev M, Madasson J and Bucher E 1999 *J. Appl. Phys.* **86** 364–9

[51] Krustok J, Raudoja J and Collan H 2001 *Thin Solid Films* **387** 195–7
[52] Krustok J, Raudoja J, Schon J H, Yakushev M and Collan H 2000 *Thin Solid Films* **361** 406–10
[53] Onishi T, Abe K, Miyoshi Y, Wakita K, Sato N and Mochizuki K 2005 *J. Phys. Chem. Solids* **66** 1947–9
[54] Eberhardt J *et al* 2005 *Thin Solid Films* **480** 415
[55] Rudigier E, Enzenhofer T and Scheer R 2005 *Thin Solid Films* **480** 327–31
[56] Dagan G, Ciszek T F and Cahen D 1992 *J. Phys. Chem.* **96** 11009
[57] Gartzman K, Chernyak L, Lyahovitskaya V, Cahen D, Didik V, Kozlovsky V, Malkovich R, Skoryatina E and Usacheva V 1997 *J. Appl. Phys.* **82** 4282
[58] Herberholz R, Rau U, Schock H W, Haalboom T, Godecke T, Ernst F, Beilharz C, Benz K W and Cahen D 1999 *Eur. Phys. J. Appl. Phys.* **6** 131
[59] Loef R, Schoonman J and Goossens A 2007 *J. Appl. Phys.* **102** 24512